Simulink modeling of an ejector based on CFD simulation

Jiachang Xue [1, a], Qinghuang Huang [2, b], Peiyong Wang [1, c] and Yichen Cai [1, d]

[1] School of Aerospace Engineering, Xiamen University, Xiamen, 361005, China

[2] School of Aviation, Liming Vocational University, Quanzhou, 362007, China

[a] xmuxjc@163.com, [b] 271852256@qq.com, [c] peiyong.wang@xmu.edu.cn,

[d] 631258214@qq.com

Abstract. A modeling and simulation study is conducted on a supersonic ejector. CFD simulations are carried out to examine the performance of the ejector, considering water vapor in the secondary flow. First, the study investigates how the composition variation of the secondary flow affects its static pressure. It is shown that when the molecular weight of the secondary flow goes up, the static pressure of the secondary flow goes down. If the water vapor is ignored in the secondary flow, the static pressure of the secondary flow changes by -4.5%. The simulation results demonstrate that the static pressure of the secondary flow normally increases with the secondary flow rate and outlet pressure and decreases with the total pressure of the primary flow. However, when the outlet pressure is too low or the secondary flow rate is too high, the static pressure of the secondary flow increases with the total pressure of the primary flow. Based on the CFD simulation data, a Simulink model for predicting the static pressure of the secondary flow is developed. Compared with the original CFD date, the maximum relative error of the Simulink prediction is -1.08%, indicating good accuracy of the Simulink model.

Keywords: Modeling and Simulation; Ejector; Altitude Ground Test Facility.

1. Introduction

AGTF (Altitude Ground Test Facility) is a key system in developing aero engines, and to meet the testing requirements of advanced engines in the future, countries worldwide have invested considerable resources in constructing AGTF and actively developing modeling and simulation technologies for flight environment simulation systems (FESS). Montgomery et al.[1-3] showed how important modeling and simulation were in engine testing. They studied the test facility modeling at the Arnold Engineering Development Center (AEDC) and developed simulation software. Bierkamp et al.[4] developed a simulation platform that integrated an AGTF and its control system. In 2013, Weisser et al.[5] designed a hardware-in-the-loop (HIL) simulation platform for the FESS of an AGTF. They also investigated the feedforward control technique for intake pressure. Butler et al.[6] researched the simulation system for the fuel heating system at an aerodynamics and propulsion test facility based on models of the control valve and pipeline. Zhou et al.[7] developed the temperature and pressure models for the pressure regulation chamber, the mass flow rate model of the control valve, and the HIL simulation system. Pei et al.[8-10] proposed a quasi-one-dimensional flow modeling approach for an AGTF. They analyzed the facility's dynamic control features and developed a model library with control valves, pipeline cavities, and hydraulic servo systems. They also created and validated a numerical simulation model for the FESS.

Supersonic ejectors are important parts of AGTF exhaust systems. They use high-pressure gas to pull low-pressure gas and create an environment with low pressure. They are frequently used in cooling, propulsion, water treatment, and thermal energy recovery.[11] CFD is recognized as a reliable tool for simulating the flow characteristics of ejectors[12]. Mazzelli et al.[13] showed that the SST k-ω model usually gives a better prediction of the mass flow rate, as well as the ejection ratio. Liang et al.[14] utilized a combined approach of numerical simulation and experiment to reveal the overall performance of the precooled ejector with a heat exchanger. They also study the effect of the secondary flow conditions on the ejector's performance. Hou et al.[15] used CFD to study how the molecular weight of the secondary flow affected the ejector's performance and then created a

regression model for the ejection ratio.

Currently, simulation and modeling research on exhaust systems of AGTF is incomplete, particularly lacking research on secondary flow characteristic analysis with large water vapor concentration. In order to promote the development of advanced simulation technologies, it is necessary to establish a complete Simulink model library. The present study focuses on a supersonic ejector within an AGTF exhaust system. The CFD simulation calculates the flow field with large water vapor in the secondary flow. The study investigates how and why the change in the gas composition of the secondary flow affects the pressure. Additionally, it explores the influence of the secondary mass flow rate, the total pressure of the primary flow, and the outlet pressure on the pressure of the secondary flow. Finally, a Simulink model is developed for the ejector based on the simulation data.

2. CFD simulation

The ejector structure is shown in Figure 1(a). There are two inflows: the blue arrow indicates the low-pressure secondary flow, which is the high-temperature exhaust from the engine after cooling through water evaporation, and the red arrow indicates the primary flow, which is medium-pressure air. In the converging-diverging nozzle, the air changes its pressure energy into kinetic energy, creating a supersonic, low-pressure flow that guides the secondary flow into the mixing section. The purple arrow indicates the mixed flow. The mixing section mixes the primary and secondary flows, facilitating momentum and energy exchange. Then, the mixture flows out of the ejector. Figure 1(b) shows the structure and size of the converging-diverging nozzle.

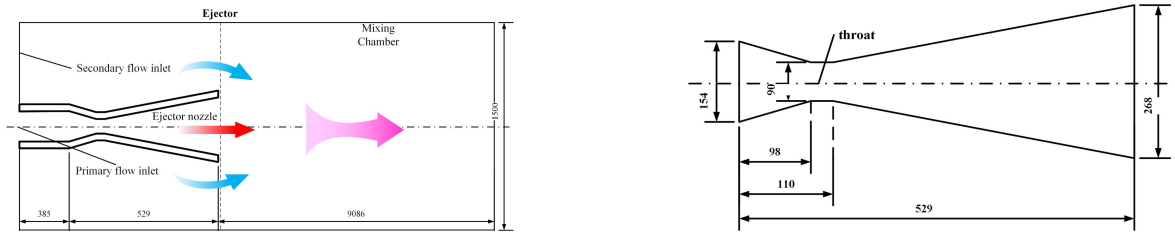

(a) (b)

Figure 1. Structure and size: left, ejector schematic; right, converging-diverging nozzle

Due to geometric and physical axisymmetry, two-dimensional axisymmetric CFD simulations are used to study the flow field of the ejector. The primary flow inlet is set as a stagnation inlet, the total temperature is fixed at 300 K, and the fluid is air (N_2 and O_2 mole ratio 0.79:0.21). The total pressure is set to [3000, 4000, 5000, 6000] KPa. The secondary flow inlet is set as the mass flow inlet, the total temperature is fixed at 500 K, and the gas composition will be described later. The range for the mass flow rate is [5-80] with a 5 Kg/s interval. The outlet is set as the pressure outlet, the pressure value is adjusted to [20, 40, 60, 80, 100] KPa, the axis is the central axis of the ejector, and the remaining surfaces are set as adiabatic walls. Figure 2 shows the generated mesh. The number of meshes is about 160,000. Further increasing the number of meshes has almost no effect on the simulation result.

The flow is a steady, compressible, turbulent, and multi-species (N_2, O_2, CO_2, H_2O) flow. The ideal gas law calculates the density of the mixture; the turbulence model uses the SST k-ω model and all Y^+ wall treatment. The physical parameters of each species, including the specific heat, viscosity, and conductivity, are all functions of temperature. The specific heat and enthalpy use the NASA 14 coefficient polynomials, while the other parameters are in CHEMKIN format. The properties of the mixture are calculated using the mixture averaging rule.

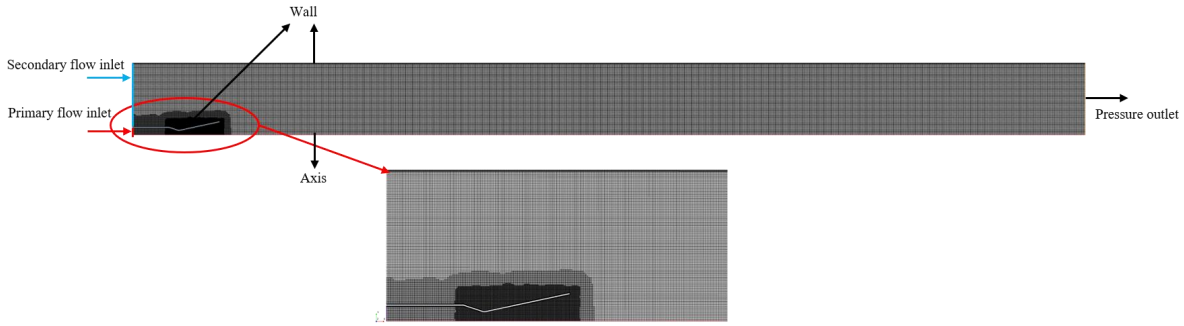

Figure 2. Two-dimensional mesh of ejector

3. Results and discussion

An example of the simulation is given for illustration. The primary flow total pressure is 4000 KPa. The mass flow rate of the secondary flow is 75 Kg/s, and the gas is the cooled exhaust gas whose composition is N_2, H_2O, O_2, and CO_2, with the molar fractions of 44.71%, 45.41%, 5.94%, and 3.94%, respectively. This composition is calculated based on the cooling of an aero-engine exhaust to 500 K with cold water. The outlet pressure is set to 40 KPa. The mass flow average pressure at the secondary flow inlet is monitored, and the calculated value is 36.86 KPa. The Mach number and temperature contours of the simulation are shown in Figures 3 and 4.

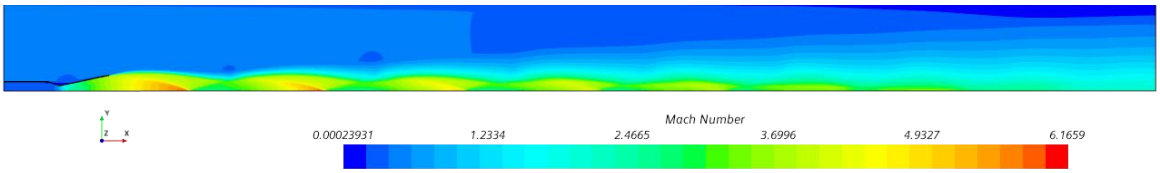

Figure 3. Simulated Mach number contour

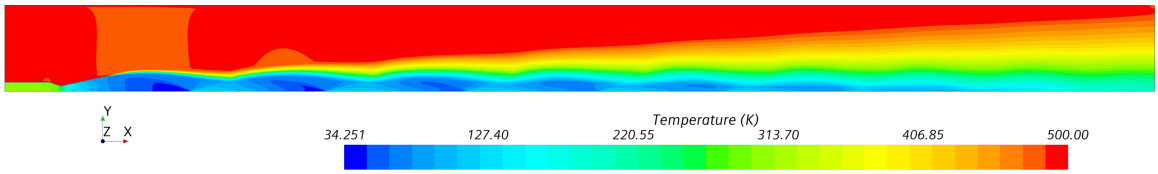

Figure 4. Simulated temperature contour

According to Figs. 3 and 4, the converging-diverging nozzle accelerates the primary flow, reaching Ma = 1 at the nozzle throat, and the gas continues to accelerate, reaching a supersonic speed in the divergent section of the nozzle. The gas expands further outside the nozzle, then a series of shock waves are generated. The ejection of the hypersonic flow accelerates the secondary flow, and a strong shear layer is formed between the primary and secondary flows in the mixing section. This shear layer is the core region of the mixing, and the mixture flows out of the ejector at a high speed finally. To examine the effect of water vapor, the simulation is run with different secondary flow compositions while other conditions remain the same. Table 1 shows the simulation result with the exhaust gas only (molar fractions of N_2, H_2O, O_2, and CO_2 are 76.29%, 6.84%, 10.14%, and 6.73%, respectively).

It can be seen in Table 1 that the gas composition has some effect on the secondary flow

pressure. With water vapor in the secondary flow, the molecular weight of the gas is lower. Since the secondary mass flow rate is constant, a higher molecular weight increases the secondary flow density and decreases the speed. Under the same primary flow total pressure and outlet pressure conditions, the ejector has a better pumping effect for the secondary flow with lower speed. So, the secondary flow's pressure and total pressure decrease. Compared to the exhaust gas with water vapor, the static pressure without water vapor decreases by 4.5%.

Table 1. Simulation data of secondary flow inlet corresponding to different gas compositions

	Molecular weight (g/mol)	Velocity (m/s)	Total pressure (KPa)	Static pressure (KPa)
Exhaust gas with H_2O	24.34	193.51	41.19	36.86
Exhaust gas	28.81	171.29	39.02	35.20

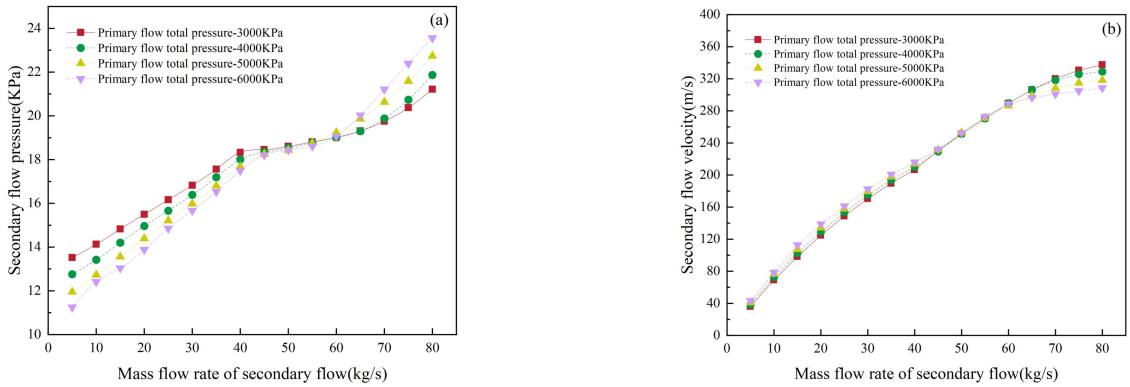

Figure 5. Simulated inlet data of secondary flow with different secondary mass flow rates and primary flow total pressure: a, inlet static pressure; b, inlet velocity

The exhaust gas with water vapor is further studied as the secondary flow composition. When the outlet pressure is reduced to 20 KPa, the effect of the secondary mass flow rate and the primary flow total pressure on the static pressure of the secondary flow is discussed. Figure 5(a) shows that as the mass flow rate of the secondary flow increases, the secondary flow pressure increases. When the secondary flow rate is less than 45 Kg/s, increasing primary flow pressure decreases the secondary pressure, which is a normal phenomenon for an ejector. However, when the secondary flow rate is more than 65 Kg/s, the secondary pressure increases with the primary pressure, which is an abnormal phenomenon for an ejector. The Mach number contours for the secondary flow with 20 Kg/s and 75 Kg/s flow rates are shown in Fig. 6 to explain the difference. At the mass flow rate of 75 Kg/s, the secondary flow is accelerated to supersonic in the ejector; however, the secondary flow will always be subsonic no matter what the primary flow total pressure is at the 20 Kg/s secondary mass flow rate. The supersonic flow of the secondary flow means the secondary flow is choked; as the primary pressure increases, the first expansion wave is larger, meaning the throat of the secondary flow passage is compressed to have less area. To keep the secondary flow rate constant, the inlet pressure must be raised.

The secondary flow pressure variation with the secondary flow rate and primary pressure at the outlet pressures of 40 Kpa and 60 Kpa is shown in Fig. 7. It is clearly seen that the ejector is running in the normal mode, i.e., the secondary pressure decreases with primary pressure. Increased outlet pressure increases the overall pressure level. Under a fixed secondary mass flow rate, the

secondary flow velocity decreases, and the secondary flow never accelerates to supersonic flow in the tested secondary flow rate range. Of course, further increase of the secondary flow rate can still make the secondary flow supersonic, and the abnormal phenomenon of the secondary flow pressure happens again.

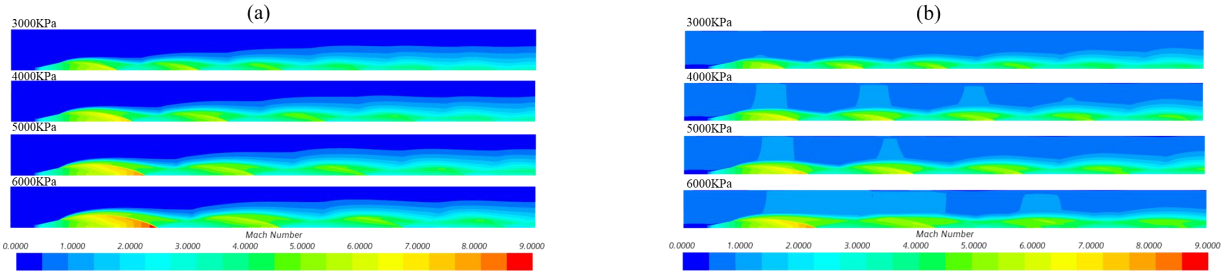

Figure 6. Simulated Mach number contours with different primary flow total pressure (outlet pressure 20 KPa) and secondary flow rates: a, 20 Kg/s; b, 75 Kg/s

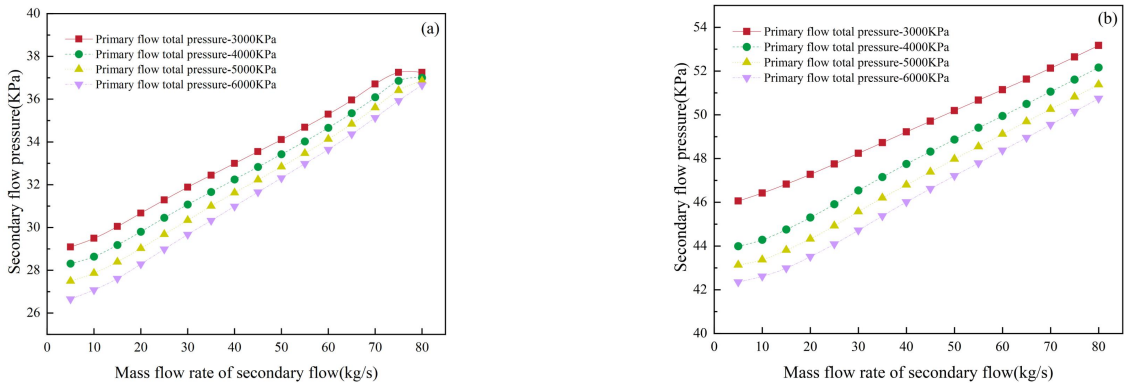

Figure 7. Secondary flow pressure corresponding to different outlet pressure: a, 40kPa; b, 60kPa

Figure 8 shows the Simulink model for the secondary flow pressure prediction of the ejector, obtained by combining all the simulation data into the Simulink n-D Lookup Table block. The input parameters are the primary total pressure, the ejector outlet pressure, and the secondary mass flow rate. Then, the secondary flow pressure is predicted by interpolation. In order to verify the reliability of the model, the operating conditions shown in Table 2 are used to calculate secondary flow pressure in the Simulink model and the CFD simulation, respectively. The maximum relative error between them is -1.08%, which means the Simulink model is accurate.

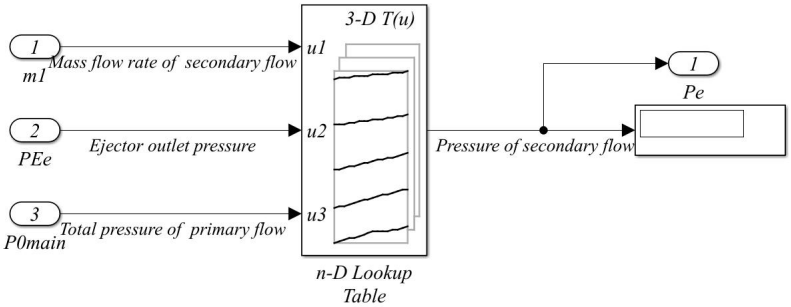

Figure 8. Simulink model for predicting secondary flow static pressure

Table 2. Predicted secondary static pressure comparison between CFD and Simulink model

	Secondary mass	Primary flow total	Outlet	Simulink	CFD	Relative

	flow rate (Kg/s)	pressure (KPa)	pressure (KPa)	(KPa)	(KPa)	error (%)
Case1	22.5	4500	50	37.43	37.35	0.21
Case2	67.5	5500	70	57.37	57.29	0.14
Case3	77.5	3500	20	21.05	21.28	-1.08

4. Conclusion

A CFD simulation study is carried out for an AGTF ejector; the analysis of the results supports the following findings. Parameters at the secondary flow inlet are affected by the secondary flow gas composition. An increase in the molecular weight of the secondary flow will lead to an increase in the secondary flow density and a decrease in the velocity and static pressure. Accurate composition in the CFD simulation should be used to obtain accurate data. The variation of the secondary flow pressure with the secondary flow mass flow rate, the primary flow total pressure, and the outlet pressure are analyzed. When the secondary flow rate is too high or the outlet pressure is too low, the secondary flow pressure could increase with the primary flow pressure since the secondary flow is choked in the ejector, and the larger primary pressure will compress the throat area of the secondary flow passage. This kind of operation state should always be avoided. A Simulink model for the secondary flow pressure prediction of the ejector is built based on the n-D Lookup Table block using the CFD simulation data, and its prediction accuracy is validated with the original CFD data. The maximum relative error of -1.08% indicates that the modeling method is reasonable, thereby enriching the mechanism model library of the AGTF. It can be applied in constructing the AGTF simulation platform.

References

[1] Montgomery P.A., Burdette R. and Krupp B. (2000) A Real-Time Turbine Engine Facility Model and Simulation for Test Operations Modernization and Integration. In: ASME Turbo Expo 2000: Power for Land, Sea, and Air.

[2] Davis M. and Montgomery P. (2002) A Flight Simulation Vision for Aeropropulsion Altitude Ground Test Facilities. In: ASME Turbo Expo 2002: Power for Land, Sea, and Air. pp. 21-31.

[3] Montgomery P.A., Burdette R., Klepper J. and Milhoan A. (2002) Evolution of a turbine engine test facility to meet the test needs of future aircraft systems. In: Turbo Expo: Power for Land, Sea, and Air. pp. 119-128.

[4] Bierkamp J., Ko¨cke S., Staudacher S. and Fiola R. (2007) Influence of ATF Dynamics and Controls on Jet Engine Performance. In: ASME Turbo Expo 2007: Power for Land, Sea, and Air. pp. 105-113.

[5] Weisser M., Bolk S. and Staudacher S. (2013) Hardware-In-The-Loop-Simulation of a Feedforward Multivariable Controller for the Altitude Test Facility at the University of Stuttgart. In: Deutscher Luft- und Raumfahrtkongress Stuttgart. pp.

[6] Butler K. (2014) Upgrades to the Aerodynamic and Propulsion Test Unit Heated Fuel System (Invited). In: 19th AIAA International Space Planes and Hypersonic Systems and Technologies Conference.

[7] Zhou J., Shen L. and Zhang T. (2016) Modeling and HIL Simulation of Flight Conditions Simulating Control System for the Altitude Test Facility. International Journal of Turbo & Jet-Engines, 33.

[8] Pei X., Zhang S., Dan Z., Zhu M., Qian Q. and Wang X. (2019) Study on digital modeling and simulation of altitude test facility flight environment simulation system. J. Propul. Technol, 40: 1144-1152.

[9] Zhu M., Wang X., Pei X., Zhang S., Dan Z., Miao K., Liu J. and Jiang Z (2020) Multi-volume fluid-solid heat transfer modeling for flight environment simulation system. Journal of Propulsion Technology, 41: 2848.

[10] Pei X., Liu J., Wang X., Zhu M., Zhang L. and Dan Z. (2022) Quasi-One-Dimensional Flow Modeling for Flight Environment Simulation System of Altitude Ground Test Facilities. Processes, 10.

[11] Yadav S.K., Pandey K.M. and Gupta R. (2021) Recent advances on principles of working of ejectors: A review. Materials Today: Proceedings, 45: 6298-6305.

[12] Tashtoush B.M., Moh'd A A.-N. and Khasawneh M.A. (2019) A comprehensive review of ejector design, performance, and applications. Applied Energy, 240: 138-172.

[13] Mazzelli F., Little A.B., Garimella S. and Bartosiewicz Y. (2015) Computational and experimental analysis of supersonic air ejector: Turbulence modeling and assessment of 3D effects. International Journal of Heat and Fluid Flow, 56: 305-316.

[14] Liang T, Xu W., Li Z., Zhang S., Li G., and Zhang D. (2024). The starting and operating characteristics of the precooled supersonic ejector. Acta Aeronautica et Astronautica Sinica, 1-18.

[15] Hou M., Chen F. and Xia Z. (2024) Effect of secondary flow relative molecular mass on the performance of the ejector for PEMFC anode system: A quantitative analysis. International Journal of Green Energy, 21: 1447-1462.